Colloidal quantum dots decorated micro-ring resonators for efficient integrated waveguides excitation

Jean-Claude Weeber, Gérard Colas-Des-Francs, Alexandre Bouhelier, Aymeric Leray, Kirill Vasilev, Xiao Yu, Kamal Hammani, Juan-Miguel Arocas, Grégory Gadret, Laurent Markey, et al.

Research article

Jean-Claude Weeber*, Gérard Colas-des-Francs, Alexandre Bouhelier, Aymeric Leray, Kirill Vasilev, Xiao Yu, Kamal Hammani, Juan-Miguel Arocas, Gregory Gadret, Laurent Markey and Benoit Dubertret

Colloidal quantum dots decorated micro-ring resonators for efficient integrated waveguides excitation

https://doi.org/10.1515/nanoph-2019-0516
Received December 12, 2019; revised March 8, 2020; accepted March 24, 2020

Abstract: Micro-ring resonators made of titanium dioxide were decorated with local light sources comprising CdSe/CdS colloidal quantum dot aggregates. The active micro-resonators are operated to achieve efficient evanescent excitation of nearby co-planar integrated waveguides. Coupled-mode analysis and numerical simulations are used to capture the dynamic of the optical interaction between locally activated resonators and integrated waveguides. In this context, we exemplify the key role of resonator intrinsic loss. Next, we show that locally activated or bus-waveguide excited resonators are in optimum waveguide interaction for the same so-called critical coupling condition, although the physical origin of this property is different for each configuration. More importantly, we found that a locally activated resonator is a fabrication imperfection tolerant configuration for the coupling light of local sources into waveguides. This remarkable property originates from the opposite change of the power cycling into the resonator and the waveguide coupling efficiency as a function of the resonator-waveguide separation gap. By operating an 8-μm-radius ring resonator with loaded quality factors around $Q=2100$, we experimentally demonstrate a 5.5-dB enhancement of the power coupled into the output waveguide compared to a direct local source waveguide excitation.

Keywords: colloidal emitters; micro-ring resonator; local light sources; titanium dioxide waveguide; integrated light source resonators.

1 Introduction

Integrated traveling wave resonators (TWRs) such as micro-ring or micro-disks are often operated for on-chip filtering purposes. The classical TWR excitation configuration relies on evanescent coupling with the modes of a nearby placed bus waveguide [1]. Triggered by the development of on-chip quantum light sources, the excitation of integrated TWR by single emitters has mostly been considered recently by operating solid state quantum emitters [2, 3] or even organic emitters [4]. At a more practical level, many emitters interacting with integrated TWRs [5] are relevant for classical light sources. For example, lasing under continuous optical pumping has been demonstrated by integrating colloidal quantum dots (QDs) into SiN micro-disks [6]. Monolithic micro-ring lasers directly made of colloidal QDs have also been reported [7, 8]. Owing to the improvement of emission properties of colloidal QDs, nowadays it is clear that combining integrated devices with colloidal QDs is a relevant and versatile approach for the development of low cost optically active devices [9, 10]. In this context, not only laser sources are of practical interest. Indeed, for applications targeting bio-sensing, for example, broadband incoherent light sources relying on QDs fluorescence are already useful [11]. Whatever the targeted applications, colloidal QD light sources are only of interest if efficiently coupled to the

***Corresponding author: Jean-Claude Weeber,** Laboratoire Interdisciplinaire Carnot de Bourgogne, UMR 6303 CNRS-Université de Bourgogne-Franche Comté, 9 avenue A. Savary, F-21078 Dijon, France, e-mail: jcweeber@u-bourgogne.fr. https://orcid.org/0000-0002-9450-2962
Gérard Colas-des-Francs, Alexandre Bouhelier, Aymeric Leray, Kirill Vasilev, Xiao Yu, Kamal Hammani, Juan-Miguel Arocas, Gregory Gadret and Laurent Markey: Laboratoire Interdisciplinaire Carnot de Bourgogne, UMR 6303 CNRS-Université de Bourgogne-Franche Comté, 9 avenue A. Savary, F-21078 Dijon, France. https://orcid.org/0000-0002-0391-2836 (A. Bouhelier)
Benoit Dubertret: Laboratoire de Physique et d'Étude des Matériaux, Centre National de la Recherche Scientifique, UMR8213, École Supérieure de Physique et de Chimie de la ville de Paris, 10 Rue Vauquelin, 75231 Paris, France

on-chip photonic circuit. Beyond randomly distributed QDs around waveguides [12] or encapsulation into waveguides [13–17], placing QDs in a controlled way in weak interaction with an optical cavity offers the opportunity to tailor their emission properties by means of the Purcell effect [18–20]. However, one should not only consider QD coupling to cavity modes but also controlled light extraction from the cavity to the photonic circuitry. In this work, we focus on light coupling from a locally excited micro-resonator to an output waveguide. More specifically, we investigate the excitation of ridge waveguides coupled to micro-ring resonators optically activated by local light sources comprising colloidal QD aggregates. The deployment of such colloidal QD light sources at the scale of resonator arrays is a first step toward the development of a new class of highly-parallel, optical alignment free, spectrally encoded, resonator-based integrated optics sensors. Beyond bio-sensing purposes, a locally excited micro-ring resonator in optical interaction with an integrated waveguide is a generic configuration that is also of interest for quantum applications provided the local light source is scaled down to the single emitter level.

Our study is organized as follows. We first derive the properties of locally activated resonators interacting with output waveguides on the basis of a coupled mode formalism. Realistic designs are next considered by numerical modeling performed with the Fourier modal method (FMM) using a line source excitation of the micro-resonators. In Section 3, we report on the experimental characterizations of micro-ring resonators excited by CdSe/CdS core-shell colloidal QD aggregates deposited at controlled locations. The fabrication process of titanium dioxide (TiO_2) micro-resonators decorated with QD aggregates is described along with the optical characterization procedure. In agreement with our modeling, we show that the optimum enhancement factor is obtained for the resonator featuring the lowest optical losses including losses originating from the scattering by the QD aggregates deposited onto the resonators. For resonators featuring moderate loaded quality factors (around 2000), we obtain a more than three-fold enhancement of the power coupled into the waveguides with the locally activated resonators as compared to direct local waveguide excitation.

2 Locally activated micro-resonators

The basic understanding of waveguide excitation by a locally activated TWRs can be first captured from a coupled-mode approach assuming a classical local light source exciting resonator modes. For a more realistic modeling of a local emitter weakly coupled to a resonator in optical interaction with an output waveguide, we apply a fully numerical method in the next paragraph.

2.1 Coupled mode formalism

Let us consider first the standard configuration of a bus waveguide coupled to a TWR [see Figure 1A].

Let E_s^+ and E_{wg}^+ be the incident and through (output) port field, respectively. By correlating those two fields to the inner resonator fields, it can be shown that the transmission power function of this "all-pass" configuration is given by [21]:

$$\frac{I_{wg}^+}{I_s^+} = \frac{r^2 + a^2 - 2ra\cos(\phi)}{1 + ra^2 - 2ra\cos(\phi)} \tag{1}$$

where $I_{wg}^+ = E_{wg}^+ E_{wg}^{+*}$, $I_s^+ = E_s^+ E_s^{+*}$ and where r is the Fresnel reflection coefficient of the interface describing the non-lossy coupling region between the resonator and the bus-waveguide. The parameters a and ϕ are the attenuation coefficient and the phase accumulated per round-trip respectively. For vanishing small optical losses, the attenuation coefficient a approaches one. At a resonant

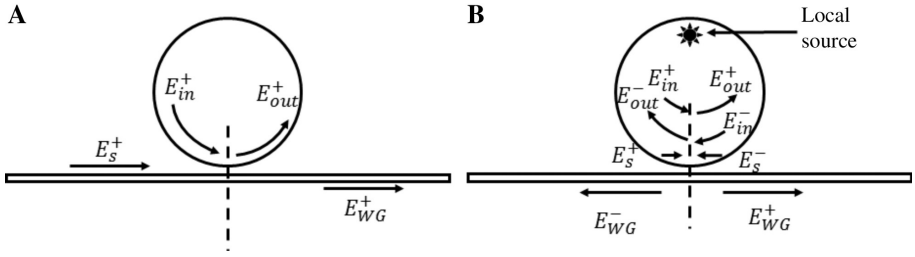

Figure 1: (A) [resp. (B)] Schematic view of a bus-waveguide excited TWR (resp. locally activated TWR).
Situation (A) corresponds to the classical bus-waveguide excitation of the resonator. The incoming field is evanescently coupled to the resonator and back to the output waveguide. In situation (B), the light source is implanted within the resonator. The local source excites contra-directional traveling modes of the resonator that couple back into the output waveguide.

frequencies ($\phi = m2\pi$ with m an integer), the through port intensity I_{wg} vanishes whenever $r = a$, a condition known as critical coupling. In practical situations, r can be adjusted by finely tuning the TWR-waveguide separation gap to achieve high extinction ratios at resonant frequencies.

We focus now on the less conventional situation depicted in Figure 1B. We assume a local source implanted into the TWR. The local source can be a quantum emitter in weak coupling interaction with the resonator or a more classical point-like source such as a point-like scatterer [22] or the probe of an illumination-mode near-field optical microscope [23]. The local source creates initial fields E_s^+ and E_s^- at the location of the virtual interaction interface (dashed line in Figure 1B) between the TWR and the waveguide. The field E_s^+ (resp. E_s^-) is incident onto the interaction interface after a partial counter-clockwise (resp. clockwise) round-trip into the TWR. In this respect, E_s^+ and E_s^- play the same role as the incident field for the bus-waveguide excitation configuration shown in Figure 1A. The clockwise (cw) and counter-clockwise (ccw) mode of the resonator are coherently built-up from those two initial fields, respectively. The simultaneous excitation of the cw and ccw mode creates a standing wave pattern nevertheless the resonator is still a TWR in nature [24]. The symmetry of the standing wave pattern (odd or even) with respect to the coupling interface is at the origin of a frequency shift of the resonances compared to an unidirectional (cw or ccw) excitation of the resonator [25]. The frequency shift originates from a non-zero back-reflection of the coupling interface allowing for a fraction of the mode power cycling in one direction to contribute to the power flowing in the opposite output port (e.g. the ccw mode contributes to the excitation of the left side output port). The frequency shift is only significant for high quality factor resonators (Q around 10^5) [26] and can be safely neglected in many practical situations. The resonators considered in the following feature moderate quality factors (around 2000) for which the frequency shift is expected to be vanishing small. Disregarding the frequency shift allows us in our model, to neglect the back-reflection of the virtual coupling interface. With this limitation, it is then sufficient to consider an unidirectional excitation of the resonator given that for initial fields E_s^+ and E_s^- of same amplitude, the net power traveling into the resonator is zero leading to an equally distributed power flow on the right and left output port. The ccw fields E_{in}^+ and E_{out}^+ on each side of the interaction interface are linked by $E_{\text{in}}^+ = a\exp(j\phi)E_{\text{out}}^+$ and $E_{\text{out}}^+ = r(E_s^+ + E_{\text{in}}^+)$. From those two equations, it is a simple matter to show that $E_s^+ + E_{\text{in}}^+ = \dfrac{E_s^+}{1 - ra\exp j\phi}$. This last equation is readily identified as the sum of a geometric series of first term E_s^+ and common ratio $ra\exp(j\phi)$ revealing the coherent build-up of the total field $E_s^+ + E_{\text{in}}^+$ by successive round-trips in the resonator starting from the initial source field E_s^+. The field E_{wg}^+ traveling along the right output waveguide is given by $E_{wg}^+ = jt(E_s^+ + E_{\text{in}}^+)$ where t denotes the Fresnel transmission coefficient from the resonator to the waveguide (and vice-versa) and where the pure imaginary factor j originates from the $\pi/2$ phase shift induced by the evanescent coupling. Assuming a non-lossy interaction interface ($r^2 + t^2 = 1$), the intensity at the through port I_{wg} normalized to the initial intensity of the source I_s is given by:

$$\frac{I_{wg}^+}{I_s^+} = \frac{1 - r^2}{1 + (ra)^2 - 2ra\cos(\phi)} \tag{2}$$

At resonance frequencies, the normalized output intensity becomes $\dfrac{I_{wg}^+}{I_s^+} = \dfrac{1 - r^2}{(1 - ra)^2}$. On maximizing this ratio against r, one finds a maximum output intensity when $r = a$. Remarkably, for a given value of the attenuation factor a, the critical coupling condition not only corresponds to the optimum extinction with bus-waveguide excitation but also to the maximum output intensity when the source is implanted into the resonator. For such an optimum critical coupling condition, the output port intensity reduces to $\dfrac{I_{wg}^+}{I_s^+} = \dfrac{1}{1 - a^2}$ suggesting very efficient waveguide excitation with low loss ($a \simeq 1$) locally activated resonators. Figure 2A shows the normalized output port intensity considering either a bus waveguide or a TWR excitation. In both cases we assume a ring resonator with an average radius of $R_{AV} = 8$ µm supporting a mode at a free-space wavelength $\lambda_0 = 670$ nm with an azimuthal order $m = 119$ corresponding to an effective azimuthal index of $n_{\text{eff}} = \dfrac{m\lambda_0}{2\pi R_{AV}}$ of 1.58. The output intensity features a pronounced dip or peak for bus waveguide or TWR excitation, respectively. For bus-waveguide excitation, the field evanescently coupled in and out the resonator accumulates a π-phase shift and interferes destructively with the field directly transmitted along the waveguide, leading to the dip at resonance frequencies. For TWR excitation, such a destructive interference path does not exist anymore and an intensity peak at resonance frequencies are observed similar to the peaks found at the drop port of an add-drop resonator configuration [27]. Figure 2B displays the normalized intensity at the through port for bus and TWR excitation at resonance

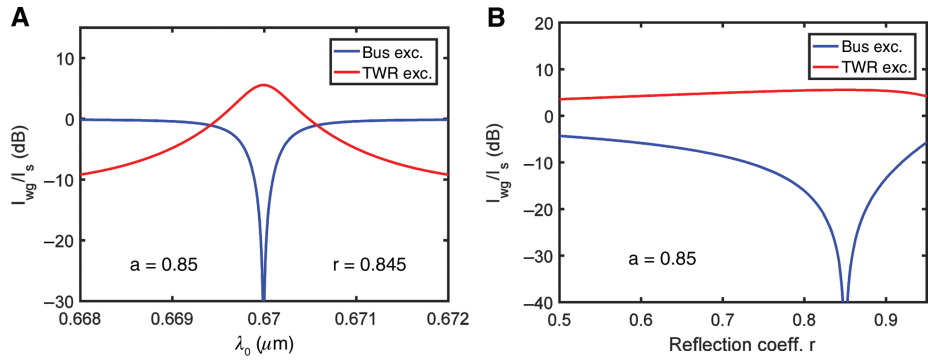

Figure 2: (A) Normalized electric field intensity coupled into the output waveguide (right port) in the case of bus-waveguide excitation and local excitation. The computation is performed at quasi critical coupling ($r \simeq a$). For bus-waveguide excitation the resonance features a sharp dip whereas a broad peak is observed for the locally activated resonator. (B) Output waveguide coupled power resonance at 670.2 nm as a function of reflection coefficient r for a fixed attenuation value of $a = 0.85$. For both configurations, resonance occurs at critical coupling ($r = a$).

($\phi = m2\pi$) when the attenuation is chosen equal to $a = 0.85$ and when r is varied. An increasing value of r corresponds to a larger amount of field kept in the resonator and can be practically realized by increasing the TWR-waveguide separation gap. While for the bus-waveguide excitation, I^+_{wg} drops abruptly at critical coupling ($r = a$), waveguide intensity for TWR excitation features a rather smooth resonance peaked at $r = a$. The weak sensitivity of the coupled intensity to reflection coefficient r can be qualitatively understood from the fact that when r increases, the power cycling into the resonator increases as well and thus compensates for the decrease of the TWR-waveguide coupling efficiency. This interpretation is supported by eq. (2) if one realizes that the power transmission coefficient given by $t^2 = (1-r^2)$ and the power build-up factor in the resonator (at resonance frequencies) given by $\|\frac{E^+_{in}}{E^+_s}\|^2 = \frac{1}{(1-ra)^2}$, respectively, decreases and increases when r increases.

Figure 3A shows the contour plot of the output intensity in the case of local resonator excitation if the coefficients r and a are both varied. At a fixed value of a, we indeed observe that the output waveguide intensity is maximum at $r = a$. However, it is also clear that for a fixed value of r, the waveguide intensity increases monotonically with a at an increasing rate when r approaches 1 [see Figure 3B]. In other words, the minimization of the intrinsic losses (scattering, absorption, and bent losses) of the resonator equipped with a local source is the primary action to conduct in order to achieve an efficient waveguide excitation. For a further optimization, the adjustment of the resonator-waveguide coupling strength (by choosing the correct separation gap) should be considered.

2.2 Fourier modal method modeling

Our goal in this paragraph is to go beyond the simple coupled-mode formalism to investigate the properties of locally excited loaded (by the output waveguide) micro-ring resonators. Such a modeling is not only of interest for design purposes but also to support the conclusions of the coupled-mode formalism. The local source we consider now is an quantum emitter in a weak coupling regime with the loaded cavity. Modeling a quantum emitter in interaction with a loaded (opened) cavity can be done by computing the electromagnetic local density of states at the location of the emitter [28] provided the quasi-normal modes of the loaded cavity are known [29, 30]. Although technically and conceptually challenging, this approach is obviously beneficial for physical interpretations as it provides expressions for the Purcell factor experienced by the emitter in direct connection with the properties of the cavity. In our case, we adopt a more practical approach relying on the computation of the power radiated by a classical dipolar source [31]. The computation of the radiated power performed with the FMM [32–34] allows us to compare directly our numerical results with our experimental measurements. The FMM relies on the computation of a scattering matrix of arbitrary shaped periodic objects [35]. By applying absorbing conditions or perfectly matched conditions at the boundaries of the computation cell, non-periodic objects can be considered as well. In order to keep reasonable computation times, we restrict our analysis to two-dimensional (2D) resonators featuring a y invariant axis [see in Figure 4A]. As described below, we perform the transition from three-dimensional (3D) real configurations to 2D computational

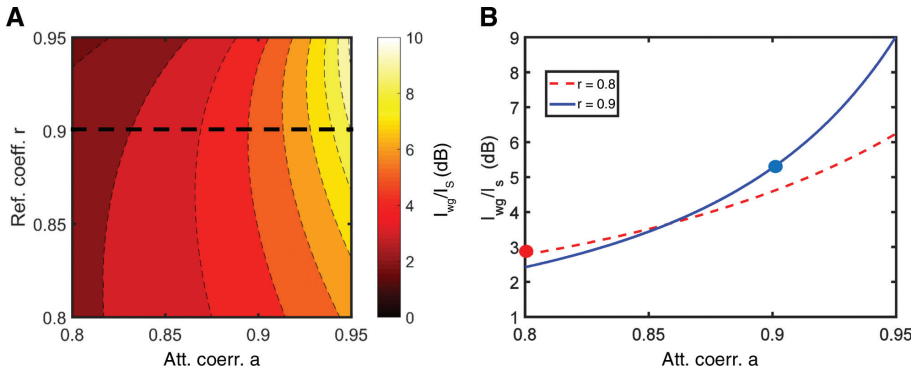

Figure 3: (A) Output waveguide coupled intensity as a function of reflection r and attenuation a coefficients. (B) Waveguide coupled intensity at fixed values of $r=0.8$ and $r=0.9$. The dot on each curve marks the critical coupling condition. For a fixed value of r, higher coupled intensities are obtained for low loss resonators ($a \to 1$) disregarding the critical coupling condition.

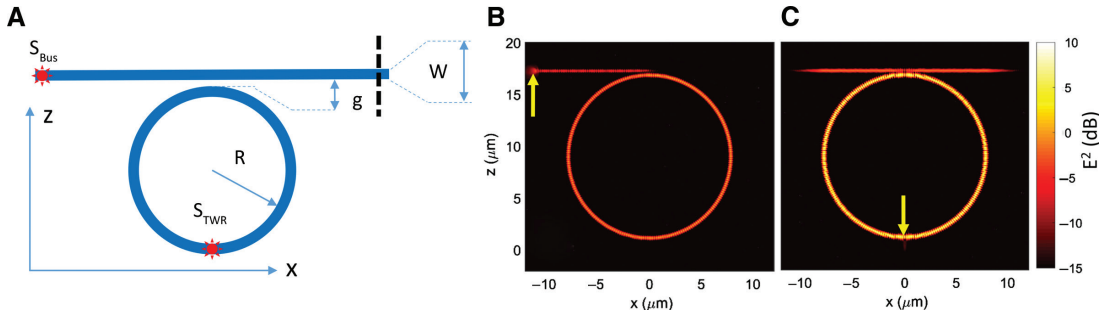

Figure 4: (A) Schematic view of the computational situation for bus-waveguide and TWR excitation configurations. (B) [resp. (C)] Electric field intensity distribution at 670.37 nm for a 8 μm radius resonator coupled to a 280 nm wide waveguide. The separation gap is $g=130$ nm. On both images, the yellow arrow shows the location of the local source.

configurations by mimicking the effective index method [36]. The plane-wave expansion of the electro-magnetic field generated in a homogeneous medium by a 2D line source located at (x_0, z_0) is given by (see page 59 in [37]):

$$A_y(x,z,t)=\frac{j}{4\pi}\int_{-\infty}^{+\infty}\frac{1}{k_z}\exp(jk_x(x-x_0))\exp(jk_z|z-z_0|)\exp(-j\omega t)dk_x \quad (3)$$

where ω is the angular frequency of the source, $k_z=\sqrt{\tilde{n}^2k_0^2-k_x^2}$ is the z-component of the wave-vector of the plane wave emitted by the source having a k_x component when the source located in a medium with a (complex) refractive index $\tilde{n}$ and $k_0=\frac{2\pi}{\lambda_0}$ with λ_0 the free-space wavelength of the monochromatic source. For a transverse electric (TE) polarized source the component A_y is the electrical field component E_y whereas A_y is identified as the magnetic field H_y in case of a transverse magnetic (TM) polarization of the field emitted by the source. From the numerical point of view, the line source is embedded in an artificial layer of vanishing thickness and eq.(3) is discretized and truncated such that $A_y(x,z,t)$ becomes:

$$A_y(x,z,t)=\frac{j}{4\pi}\sum_{-N}^{+N}\frac{1}{k_z^{(m)}}\exp(jk_x(m)(x-x_0))\exp(jk_z^{(m)}|z-z_0|)\exp(-j\omega t)\Delta k_x \quad (4)$$

where m is an integer ranging from $-N$ to $+N$ and where $k_x(m)=m\times\Delta k_x$. If sampling in k_x is chosen equal to $\Delta k_x=\frac{2\pi}{d}$ where d denotes the period of the computing cell along x, the numerical effort with the FMM for the computation of the scattered field in the presence of a local source is the same as in the case of a *single* plane wave illumination [38]. The computation situation we considered is shown schematically on Figure 4A. A micro-ring resonator of $R=8$ μm average radius (width = 280 nm) is placed in close proximity to a finite length micro-waveguide (width $W=280$ nm). The micro-ring and the waveguide are separated by a gap

g. The experiments reported in the following are conducted for TM polarized modes traveling along structures etched in a 160-nm-thick TiO_2 layer. To be consistent with this situation, our calculations are conducted by attributing to the 2D resonators and waveguides a refractive index equal to the effective index of the TM slab mode of the TiO_2 layer (around 1.76 at $\lambda_0 = 670$ nm). This approach not only allows us to take into account the thickness of our devices in our 2D calculations but also to consider dispersion of TiO_2 by adjusting the effective index of the TM slab-waveguide mode for each wavelength of interest. Note that FMM computations for the 2D situations must be conducted with TE polarized fields to model TM polarized modes sustained by 3D configurations. In this way, both TE polarized-2D and TM polarized-3D waveguiding configurations are such that the dominant electric field component is tangential to the lateral flanks of the waveguides. Finally, for subsequent computations, we place an artificial full-absorber segment at the end of the finite-length output waveguide to prevent a significant back-reflection of the forward (toward positive x values) propagating mode. The images displayed in Figure 4(B) and (C) show the electric intensity distribution at a resonant free-space wavelength of 670.37 nm for the local source located within the bus waveguide or the resonator, respectively. Both intensity distributions are normalized with respect to E_s^2, the maximum intensity produced by the local source radiating in free space. Our numerical model accounts for resonator bent losses. In order to account for extra-loss channels (such as scattering, for example), we apply an artificial non-dispersive imaginary part κ to the refractive index of the resonators. The results in Figure 4B and C were obtained with this extinction coefficient equal to $\kappa = 2\times10^{-4}$. For bus-waveguide excitation, the destructive interference leads to a vanishing signal at the output port. The intensity build-up factor into the resonator is about 4 to 5 dB. When the source is now located into the resonator, the build-up factor increases to 10 dB and the left and right output waveguides are efficiently excited.

For a more quantitative analysis, we plot in Figure 5A and B the resonance observed around 670 nm in case of bus and TWR excitation, respectively. Typical quality factor for the loaded resonator around $Q = 2500$ are obtained with $\kappa = 2\times10^{-4}$. The effect of the resonator on the output signal is evaluated relative to a reference situation where a bare waveguide (no resonator) is excited by the local source placed within the waveguide. We compute the Poynting vector flux Φ_{ref} through a relevant surface to assess the power traveling along the reference waveguide. We calculate in the same way the Poynting vector flux Φ_x at the end of the output waveguide in the case of bus-waveguide or TWR excitations. The ratio $\frac{\Phi_x}{\Phi_{ref}}$ denotes an extinction factor EF ($EF<1$) for bus-waveguide excitation and an enhancement factor (EF can be >1) for resonator-mediated excitation. Whatever the excitation configuration, EF characterizes the impact of the resonator in comparison with bare-waveguide reference situation. For bus-waveguide excitation [Figure 5A], EF is close to unity far enough from the resonance and drops below 3% (–15 dB) at resonance (670.37 nm) for gap $g = 130$ nm. For the same gap, in the case of TWR excitation [Figure 5B], we find a maximum 3.5-fold enhancement of the power at the output waveguide compared to the reference configuration. By monitoring EF for the resonance around $\lambda_0 = 670$ nm, we obtain the curve plotted in Figure 5C demonstrating the critical coupling at $g = 130$ nm. For TWR excitation [Figure 5D], maximum EF (5.4 dB) is indeed obtained for critical coupling in agreement with the conclusion of coupled-mode approach. In addition, as anticipated from the coupled mode analysis, for TWR excitation, EF depends only weakly on the separation gap. This result is of key practical interest as it indicates that TWR excitation of waveguides is robust against fabrication deviations. Finally, if κ is reduced to 1×10^{-4}, critical coupling is verified at $g = 170$ nm and a maximum enhancement factor about $EF = 7.4$ dB is obtained, the quality factor of the resonance around $\lambda_0 = 670$ nm (not shown) being in this case around 5500. Hence, we conclude once again that efficient waveguide excitation can be obtained with locally activated TWR at the cost of resonator intrinsic losses minimization. For low loss resonators, we note that a deviation from the critical coupling condition has a marginal detrimental impact on the enhancement factor EF making this configuration of key practical interest.

To conclude this numerical study, let us note that the computations have been conducted in the context of a quantum emitter in a weak interaction with a loaded cavity. In this case, the enhancement EF is interpreted in terms of the Purcell factor and the corresponding enhancement of the emitter decay rate into the loaded cavity modes as compared to the decay rate of the same emitter into waveguide modes. However, the same enhancement factors EF are also expected if, for example, a classical local source such as the tip of an illumination mode near-field optical microscope is operate to excite the resonators (provided however that the presence of the tip does not deteriorate the quality factor of the resonator). In this case, the enhancement factor EF is understood from an enhanced coupling of the near-field tip with the cavity modes and the concomitant decreases of the back reflected, absorbed, or diffracted light. In other words, the results we describe in this study hold for any kind of point-like sources (quantum emitter based in weak coupling

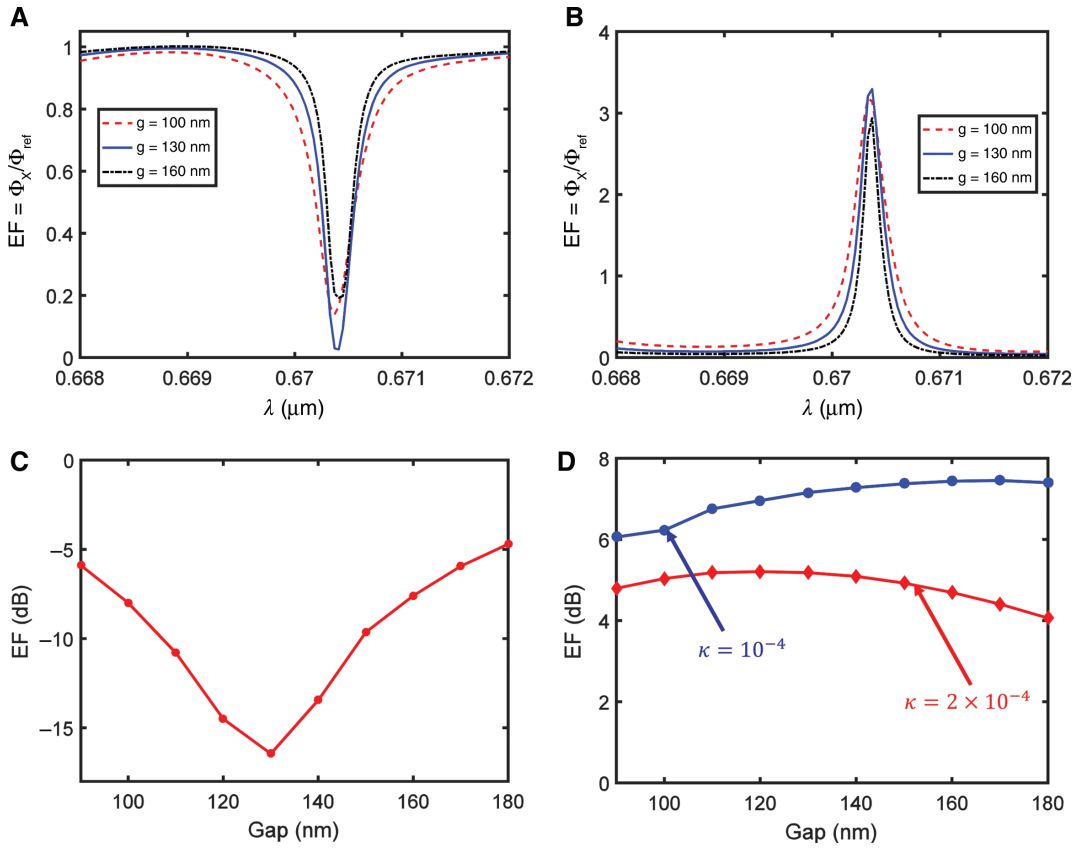

Figure 5: (A) [resp. (B)] Spectra of the power traveling along the output waveguide normalized to the power of a reference waveguide (with no resonator) in the case of bus-waveguide (resp. TWR) excitation for separation gaps of 100 nm, 130 nm, and 160 nm. The computations are conducted by imposing an extinction coefficient of $\kappa = 2\times10^{-4}$ to the refractive index of the 8 μm radius resonator.(C) Extinction factor (*EF*) (output waveguide power normalized to reference waveguide power) for bus-waveguide excitation of the resonator. The critical coupling condition is achieved for a separation gap of $g = 130$ nm ($\kappa = 2\times10^{-4}$, $Q = 2500$). (D) Enhancement factor (*EF*) (output waveguide power normalized to reference waveguide power) in the case of local TWR excitation. For an extinction coefficient of $\kappa = 2\times10^{-4}$, the enhancement factor is maximum at $g = 130$ nm corresponding to the critical coupling condition [see (C)]. By reducing resonator intrinsic losses ($\kappa = 1\times10^{-4}$, Q around 5500) the enhancement factor rises above the optimum value obtained for $\kappa = 2\times10^{-4}$ whatever the separation gap.

regime or classical local source) as long as specific emissions properties of emitters (lasing, amplified spontaneous emission…) are not involved.

3 Experimental methods

3.1 Sample fabrication and light sources deployment

The fabrication of micro-ring resonators equipped with local colloidal light sources is a two-step process. Once the integrated optics devices are obtained, the colloidal light sources must be accurately deposited at chosen locations. A TiO_2 layer is first deposited onto a 170-μm thick glass slide by sputtering of a 99.99% pure titanium target using an argon-oxygen mixture. The deposition process leads to TiO_2 mostly in anatase phase. Next, we operate an electron-beam system and a standard lift-off process to form a 25-nm thick chromium hard mask at the location of the final structures. The unprotected areas are etched by reactive ion etching using a mixture of argon and SF_6 gases at a rate of 50 nm/min. Finally, the remaining hard mask is removed by wet-etching and typical structures shown in Figure 6(A) and (B) are obtained. The structures we consider next are comprised of a waveguide (width $W = 280$ nm) coupled to an $R = 8$ μm ring resonator (width $W = 280$ nm). The gap between the waveguide and resonator is changed by a step of 10 nm from 60 nm to 140 nm. Bus waveguides are connected to grating couplers by means of a tapered waveguide. As detailed in the following, the grating coupler is intended for investigating bus-waveguide excitation of the resonators. The light sources we use in this work are colloidal CdSe-CdS core-shell quantum dot aggregates deposited onto the

integrated optics structures of interest. The deterministic deposition of the aggregates is achieved once again by electron-beam lithography following a procedure demonstrated in a previous work [39]. Figure 6C shows a low magnification scanning electron microscope (SEM) image of QD aggregates deposited onto a tapered waveguide. The aggregates appear well-defined, semi-spherical in shape with a radius around 200 nm [Figure 6D].

3.2 Optical set-up for active resonators characterizations

Optical characterizations of the samples are conducted using the set-up described in Figure 7A. It consists in an inverted microscope equipped with a high numerical aperture (100×, 1.49 NA) immersion oil objective and an up-right microscope column mounted on an accurate three-axis stepper motor stage dedicated to the illumination of the samples. The light sources we operate in the following can be either a broadband light emitting diode (LED) peaked at 680 nm or a 405-nm continuous wave (CW) low power laser diode (LD) (<100 μW). The fiber light sources (LED or LD) are moderately focused using a 10× microscope objective. The LED is used for bus-waveguide excitation configuration whereas the local QD aggregates are pumped with the 405 nm LD. QD fluorescence collected by the high-NA microscope objective is transmitted through a high-pass filter (cut-on 550 nm wavelength) and a polarization analyzer. Next the fluorescent signal is split and directed on a charge-coupled device (CCD) camera and the 10-μm wide entrance slit of a 500-mm focal

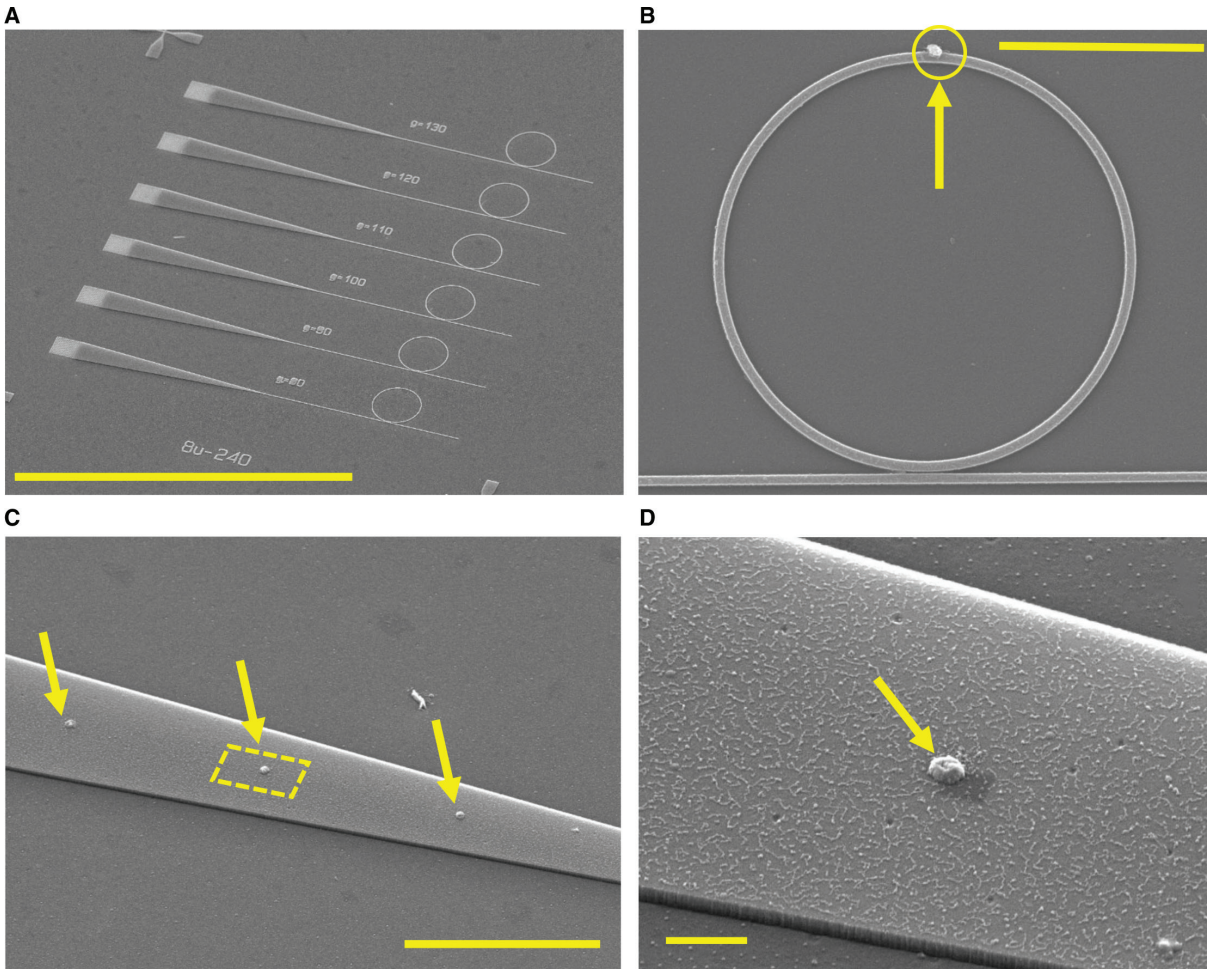

Figure 6: (A) Bird-eye view scanning electron image of the integrated TiO_2 resonators on glass (scale bar = 100 μm). The samples are comprised of grating couplers, a tapered region connected to a 280 nm-wide waveguide in interaction with ring resonators. (B) Top view SEM image of a ring resonator equipped with a CoQDs aggregate (scale bar = 5 μm). (C) SEM image of CdSe/CdS colloidal aggregates deposited at controlled locations marked by the yellow arrows (scale bar = 10 μm). (D) SEM image of the aggregate surrounded by the square perimeter in (C). The aggregate is roughly semi-spherical with a radius around 200 nm (scale bar = 1 μm).

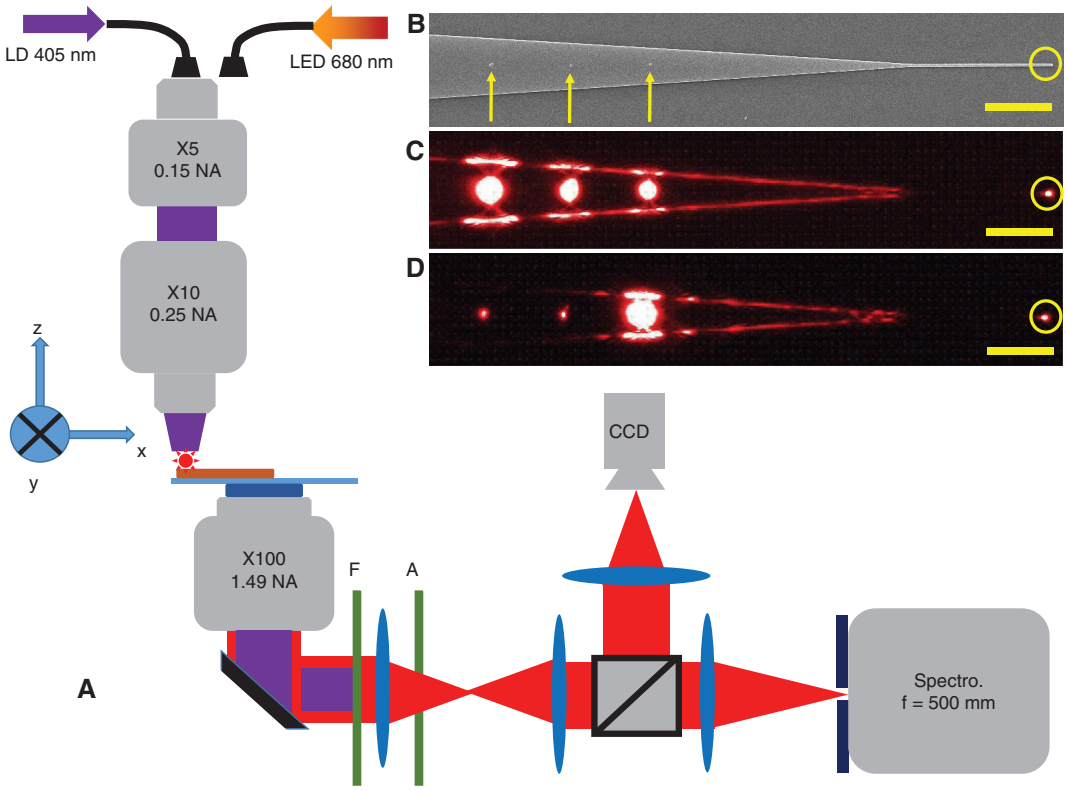

Figure 7: (A) Optical characterization set-up (F: high-pass filter, A: polarization analyzer). (B) SEM image of a tapered waveguide with three sources placed at the locations indicated by the yellow arrows. (C) [resp. (D)] fluorescent image recorded with the CCD camera in the case of collimated (resp. focused) optical pumping (at 405 nm) of the sources. The scattering spot (highlighted by a yellow circle) at the end of the waveguide demonstrates fluorescent light coupling into the waveguide. [Scale bar = 10 µm on (B), (C), and (D)].

length spectrometer fitted with a 1200 lines/mm grating. The spectral resolution of our configuration is around 70 pm. Figure 7B shows the SEM image of a tapered waveguide decorated with three QD aggregates. By defocusing the incident blue LD, the fluorescent image shown in Figure 7C is observed on the CCD camera. Apart from the light sources, one can see the edges of the tapered waveguide revealed by the scattering of the fluorescent light coupled into the waveguide. More importantly, at the exit end of the ridge waveguide a scattering spot (highlighted by yellow circle) is clearly visible. This scattering spot is still perfectly visible when the incident 405-nm LD is focused onto a single aggregate [Figure 7D]. The scattering spot at the output end of the waveguide can be detected by the high NA objective and directed onto the entrance slit of the spectrometer. The sample being mounted on three-axis piezo electric stage, an optimization of the signal collected by the spectrometer is conducted by iterative adjustment of the scattering spot relative to the spectrometer slit. We note that the signal collected by the spectrometer is emitted by a region below 1 µm in length along the waveguide (for a perpendicular orientation of the spectrometer slit relative to the waveguide). In this way, the signal at the scattering spot is characteristic of the fluorescent light coupled into the waveguide and contains a marginally small contribution from free space traveling fluorescent light.

3.3 Optical characterizations of locally activated ring resonators

Resonators equipped with local colloidal light sources have been fabricated according to the process described. Figure 8A displays a white light optical transmission image of one of the resonator. A QD aggregate is deposited onto the resonator at the location marked by the yellow arrow [see Figure 8A]. Under optical microscopy inspection, QD aggregates are perfectly visible and up to 80% of the resonators are equipped with light sources. Under cw 405-nm LD pumping, the QD aggregate generates an intense fluorescent spot but also a very neat excitation of the resonator and eventually light injection into the waveguide as shown by the intense exit end scattering spot

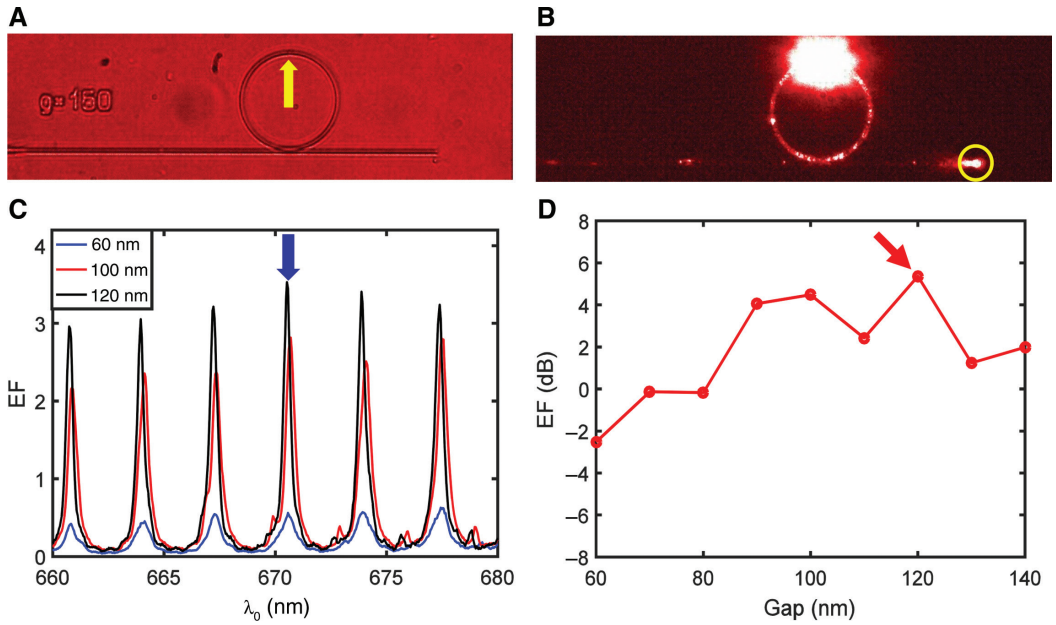

Figure 8: (A) Optical microscopy image of a resonator decorated with a colloidal QD aggregate deposited at the location shown by the arrow. (B) Fluorescent image showing the local activation of the resonator, and the scattering spot at the output waveguide end. (C) Enhancement factor spectra (reference taken from bare waveguide with no resonator) obtained for different separation gaps. Typical quality factor of the resonance around 2000–2500. (D) For the resonance close to 670 nm, enhancement factor of the output waveguide intensity spot relative to reference bare waveguides for increasing separation gaps.

[see Figure 8B]. The QD aggregates deposited on top of the resonators overlap significantly the modal field of both TE and TM polarized modes of the resonators and therefore the deposited QD aggregates allow for simultaneous excitation of both polarization modes. We separate the two contributions by polarization analysis. In all the following, we restrict our discussion to the results obtained under TM analysis corresponding to TM polarized modes traveling within the output waveguide (dominant electric field component perpendicular to the substrate surface and hence parallel to vertical waveguide flanks). Spectral analysis of the TM polarized light collected at the end of the bus waveguide leads to the spectra plotted in Figure 8C. Some residual contributions of TE polarized resonances are also observed on those spectra. Indeed, polarization filtering of the light scattered at the output port can be incomplete if light scattering occurs perpendicular to the waveguide axis. However, given that TE contributions are of small amplitude and do not overlap with TM peaks, they do not impact the analysis of the TM spectra. At this stage, it is necessary to detail the procedure used to obtain the spectra of Figure 8. The signal recorded at the output waveguide end is first normalized to the total fluorescent power collected by the high NA objective and measured with a sensitive powermeter placed on the detection path of our microscope. It is reasonable to assume that this total power (in the range of 10 nW in our case) is proportional to the power that the source can delivered to the micro-ring resonator. Thus, this total power normalization procedure is needed to perform quantitative comparison of spectra recorded on different structures equipped with different sources. The same normalization procedure applied to bare reference waveguides (with no resonator) equipped with local sources deposited at their entrance leads to an average reference spectrum characterizing the efficiency of colloidal sources for direct waveguide excitation. Finally, the comparison of bare waveguide reference spectrum with the normalized spectra collected at the output port of the QD activated ring resonator configurations allows us to assess quantitatively the added-value of locally activated resonators for waveguide excitation. In this respect, our experimental results can be compared to the numerical results of the previous sections. The enhancement factor displayed in Figure 8C is then relative to the reference bare waveguide. By considering the resonance at 670.5 nm, we note that *EF* increases by a factor 5 when the gap is changed from 60 nm to 100 nm and reaches a maximum of 3.5 for the resonator separated from the output waveguide by a gap of 120 nm. By compiling the results obtained for the resonance close to 670 nm for all gaps, we obtain the curve plotted in Figure 8D. The enhancement factor features a non-monotonous change

as a function of g and is maximum at 5.3 dB (×3.5) for $g=120$ nm. If we refer to the our numerical results, the unexpected non-monotonous behavior of *EF* versus g imposes a further investigation.

It is instructive to correlate the properties of locally activated micro-rings to bus-waveguide excitation of the same resonators. Bus waveguide coupling is performed by focusing a broadband LED source peaked at 680 nm onto the grating couplers [see Figure 6A]. Figure 9A shows an optical image captured with the CCD camera in the case of bus-waveguide resonator coupling. Light traveling along a bus-waveguide is clearly visible whereas light coupled into the resonator manifests itself through the scattering spot (arrow) at the location of the QD aggregate. Light coupled out from the exit end of the bus waveguide is once again collected to record the spectra. Figure 9B displays spectra obtained by detecting light coupled out of five reference bare waveguides. For each spectrum, we observe an interference pattern (period around 0.6 nm) attributed to the Perot-Fabry cavity formed by the finite length waveguides. We average those spectra to produce a reference spectrum of a bare waveguide. Similarly to the local activation situation, we normalize the spectrum of each resonator by this reference spectrum in order to extract the properties of the resonators relative to the average reference waveguide. The normalized spectra for gaps of 60 nm, 100 nm and 120 nm are shown in Figure 9C. We observe resonance dips with an extinction factor in the range of –10 dB. We emphasize that the patterns we consider here are the same as in the case of the local source activation meaning that the spectra we observe with LED illumination account for the presence of the QD aggregates onto the resonators. Once again we consider specifically the resonance close to 670 nm and we plot in Figure. 9(D) the extinction factor and the quality factor Q of the resonance dip for each gap value. *EF* is minimum at $g=80$ nm and features a non-monotonous change as a function of g. On the basis of this observation, we conclude that the configuration verifying a condition close to the critical coupling is obtained at $g=80$ nm. However, when considering

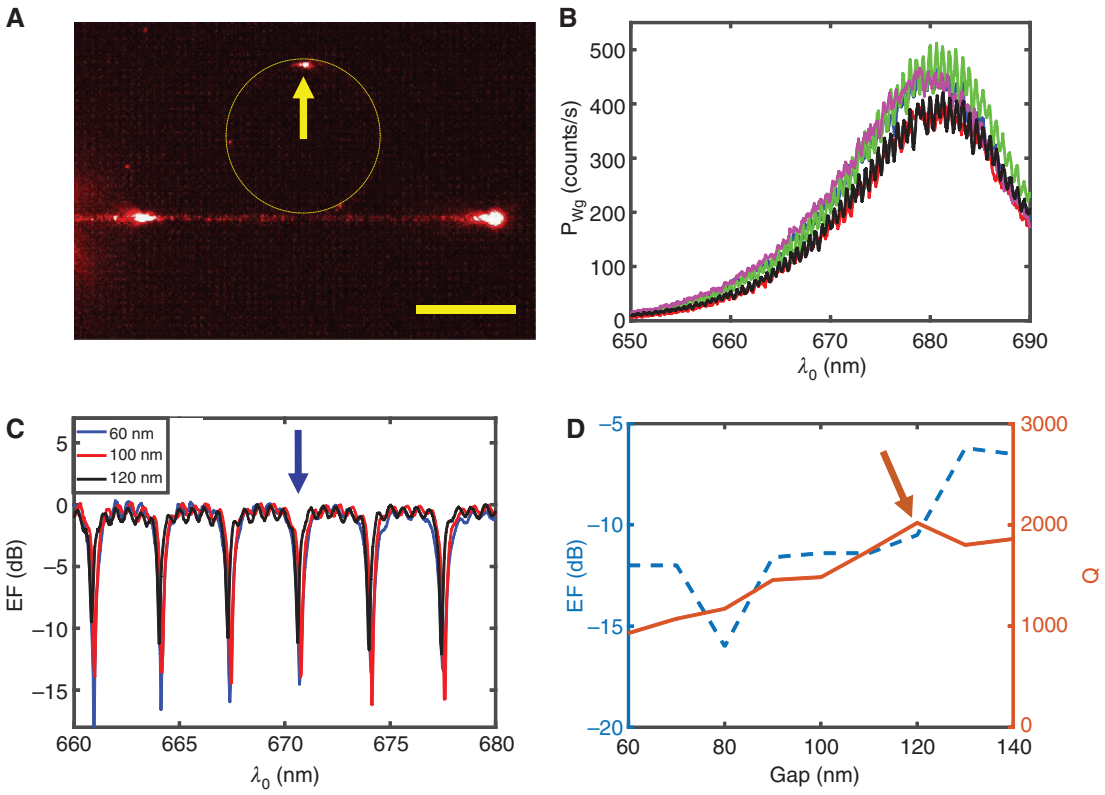

Figure 9: (A) Optical image captured on the CCD camera for bus-waveguide excitation of a resonator. The scattering spot at the location of the arrow results from scattering of light coupled in the resonator by the QD aggregate.(B) Raw spectra recorded at the end of reference bare (no-ring) waveguides. (C) Spectra recorded at the output port under bus-waveguide excitation of the resonators for different separation gaps. The spectra are plotted relative to the average reference bare waveguide spectrum. (D) Quality factor and extinction factor (relative to the average reference bare waveguide) of the dip (close to 670 nm) for different separation gaps. Gaps of $g=80$ nm and $g=120$ nm correspond, respectively, to the critical coupling condition and lowest loss configuration.

the local excitation situation [see Figure 8C], we note that this gap does not lead to any enhancement of the power coupled into the waveguide (compared to the reference waveguide) in disagreement with the numerical results discussed above. To resolve this apparent discrepancy, we consider the quality factor Q in Figure 9D and we note that once again the quality factor does not increase monotonously with increasing g as it would be expected for an ideal bus waveguide/resonator configuration. Our understanding of this behavior speculates that the quality factor of each configuration not only depends on gap g but also on losses created by each QD aggregate acting as a scatterer. Because we do not control the size of QD aggregates at the scale of few tenths of a nanometer, it is likely that the contribution of each source to resonator losses differs from one structure to the other. In such a situation, a given structure can incidentally verify critical coupling conditions (high extinction factor) and at the same time lead to a poor enhancement factor when the locally activated resonator configuration is used owing to high intrinsic losses. Indeed, as is explicitly shown by our analytical and numerical results, resonator intrinsic losses (described by attenuation coefficient a in the coupled modes approach) have a severe impact onto the enhancement factor for resonator-mediated waveguide excitation. Pushing further this interpretation, we should conclude that for reasonable gaps, the optimum enhancement factor under resonator-mediated excitation should be obtained for the lowest loss configuration. This last conclusion is actually directly supported by our experimental results. Indeed, we note that for $g=120$ nm, the highest quality factor ($Q=2100$) measured in the case of bus-waveguide coupling (indicative of a low loss configuration) also corresponds to the largest enhancement factor observed with resonator-mediated waveguide excitation, in agreement with our numerical results.

4 Conclusion

In summary, we investigated analytically, numerically, and experimentally the excitation of an integrated TiO_2 waveguide by means of a resonator equipped with a local light source. On the basis of a coupled-mode approach and numerical results, we conclude that the intrinsic attenuation of the mode within the resonator is the dominant parameter that controls the excitation efficiency of the output waveguide. For a given attenuation, the optimum coupling condition is obtained, for the so-called critical coupling. Matching the critical coupling condition is however of much less importance for resonator-mediated waveguide excitation as compared to bus-waveguide excitation of a resonator. This conclusion can be qualitatively understood from the fact that for locally excited resonators, the coherent build-up of the power within the resonator and the coupling efficiency to the output waveguide change in opposite direction versus waveguide-resonator separation gap. For example, for a locally excited resonator which is under-coupled to the output waveguide, the high power in the resonator compensates for the low amount of power delivered to the output waveguide. Ultimately, the intrinsic losses of the resonator imposes the maximum value of the power build-up factor and hence the range of the separation gap over which the resonator-waveguide configuration is effective. By deterministically depositing colloidal QD aggregates on top of integrated micro-ring resonators, we demonstrate up to three-fold enhancement of the coupled power for the resonator-mediated configuration compared to the direct excitation of the waveguides. This moderate improvement is attributed to the very large losses created by the QD aggregates acting as local scatterers on our resonators. However, based on our design rules for optimum resonator-mediated waveguide excitation, we now target an improvement of the fabrication and integration of the local sources to minimize the losses while keeping the power delivered by those sources at a sufficient level for practical applications.

Acknowledgments: JcW thanks A. Jimãnez, O. Pistoresi and S. Cuisance for technical support during the development of sample fabrication process. This work was financially supported by the french "Investissement d'Avenir" program, project ISITE-BFC (contract ANR-15-IDEX-0003). This research work has benefit from the ARCEN microfabrication platform of University of Burgundy.

References

[1] Yariv A. Universal relations for coupling of optical power between microressonators and dielectric waveguides. Electron Lett 2000;36:321–2.
[2] Elshaari AW, Zadeh IE, Fognini A, et al. On-chip single photon filtering and multiplexing in hybrid quantum photonic circuits. Nature Commun 2017;8:379.
[3] Osada A, Ota Y, Katsumi R, et al. Strongly coupled single-quantum-dot-cavity system integrated on a cmos-processed silicon photonic chip. Phys Rev Appl 2019;11:024–71.
[4] Rattenbacher D, Shkarin A, Renger J, et al. Coherent coupling of single molecules to on-chip resonators. N J Phys 2019;1:062002.

[5] Humer M, Guider R, Jantsch W, Fromherz T. Integration, photostability and spontaneous emission rate enhancement of colloidal pbs nanoscrystals for SU-based photonics at telecom wavelengths. Opt Exp 2013;21:18680–8.
[6] Xie W, Stöferle T, Rainó G, et al. On-chip integrated quantum-dot-silicon-nitride microdisk lasers. Adv Mater 2017;29.
[7] le Feber B, Prins F, De Leo E, Rabouw FT, Norris David J. Colloidal-quantum-dot ring lasers with active color control. Nano Lett 2018;18:1028–34.
[8] Rong K, Liu H, Shi K, Chen J. Pattern-assisted stacking colloidal quantum dots for photonic integrated circuits. Nanoscale 2019;11:13885–93.
[9] Geiregat P, Van Thourhout D, Hens Z. A bright future for colloidal quantum dot lasers. NPG Asia Mater 2019;11, Article number: 41.
[10] Yang Z, Pelton M, Fedin I, Talapin DV, Waks E. A room temperature continuous wave nanolaser using colloidal quantum wells. Nat Commun 2019;8.
[11] Jin L, Li M, He J-J. Optical waveguide double-ring sensor using intensity interrogation with a low-cost broadband source. Opt Lett 2013;36:1128–30.
[12] Kumar S, Bozhevolnyi S. Excitation of hybrid plasmonic waveguide modes by colloidal quantum dots. ACS Photonics 2019;6:1587–93.
[13] Prtljaga N, Coles RJ, O'Hara J, et al. Monolithic integration of a quantum emitter with a compact on-chip beam-splitter. Appl Phys Lett 2014;104:231107.
[14] Javadi A, Söllner Arcari M, Lindskov Hansen S, et al. Single-photon non-linear optics with a quantum dot in a waveguide. Nat Commun 2015;6:8655.
[15] Zadeh IE, Elshaari AW, Jöns KD, et al. Deterministic integration of single photon sources in silicon based photonic circuits. Nano Lett 2016;16:2289–94.
[16] Kim J-H, Aghaeimeibodi S, Richardson CJK, et al. Hybrid integration of solid-state quantum emitters on a silicon photonic chip. Nano Lett 2017;17:7394–400.
[17] Davanco M, Liu J, Sapienza L, et al. Heterogeneous integration for on-chip photonic circuits with single quantum dot devices. Nat Commun 2017;8:889.
[18] Zhang Y, Zeng C, Danping L, et al. Enhanced light emission from ge quantum dots in photonic crystal ring resonator. Opt Express 2014;22:12248–54.
[19] Ding D, Pereira MCL, Bauters FJ, et al. Multidimensional Purcell effect in an ytterbium-doped ring resonator. Nat Photonics 2016;10:385–8.
[20] Diguna LJ, Tjahjana L, Darma Y, Zeng S, Wang H, Birowosuto MD. Light-matter interaction of single quantum emitters with dielectric nanostructures. Photonics 2018;5:14.
[21] Heebner J, Grover R, Ibrahim TA. Optical microresonators. London: Springer-Verlag, 2008.
[22] Pan F, Smith KC, Nguyen HL, Knapper KA, Masiello DJ, Gold-Smith RH. Elucidating energy pathways through simultaneous measurement of absorption and transmission in a coupled plasmonic-photonic cavity. Nano Lett 2020;20:50–8.
[23] le Feber N, Rotenberg N, Kuipers L. Nanophotonic control of circular dipolar emission. Nat Commun 2015;6:6695.
[24] Manolatou C, Khan MJ, Shanhui F, et al. Coupling of modes analysis of resonant channel add-drop filters. IEEE J Quantum Electron 1999;35:1322–31.
[25] Čtyroký J, Richter I, Šiňor M. Dual resonance in a waveguide-coupled ring. Opt Quant Electron 2006;38:781–97.
[26] Blaize S, Gesuele F, Stefanon I, et al. Real-space observation of spectral degeneracy breaking in waveguide-coupled disk microresonator. Opt Lett 2010;35:3168–70.
[27] Van V. Optical microring resonators, theory, techniques and applications. Boca Raton, FL: CRC Press, 2017.
[28] Hümmer T, García-Vidal FJ, Martín-Moreno L, Zueco D. Weak and strong coupling rehimes in plasmonic qed. Phys Rev B 2013;87:115419.
[29] Kristensen PT, Rosenkrantz de Lasson J, Gregersen N. Calculation, normalization and perturbation of quasinormal modes in coupled cavity-waveguide systems. Opt Lett 2014;39:6359–62.
[30] Lalanne P, Yan W, Sauvan C, Hugonin J-P. Light interaction with photonic and plasmonic resonances. Laser Photonics Rev 2018;12:1700113.
[31] Archambault A, Marquier F, Greffet J-J, Arnold C. Quantum theory of spontaneous and stimulated emission of surface plasmons. Phys Rev B 2010;82:035411.
[32] Lalanne P, Silberstein E. Fourier modal methods applied to waveguide computational problems. Opt Lett 2000;25:1092–4.
[33] Silberstein E, Lalanne P, Hugonin J-P, Cao Q. Use of grating theories in integrated optics. J Opt Soc Am A 2001;18:2865–75.
[34] Hugonin J-P, Lalanne P, Del Villar I, Matias I. Fourier modal methods for modeling optical dielectric waveguides. Opt Quant Electron 2005;37:107–19.
[35] Li L. Formulation and comparison of two recursive matrix algorithms for modeling layered diffraction gratings. J Opt Soc Am A 1997;13:1024–34.
[36] Okamoto K. Fundamentals of optical waveguides. London: Springer-Verlag, 2006.
[37] Chew WC. Waves and fields in inhomogeneous media. New York: IEEE Press, Inc., 1995.
[38] Rigneault H, Lemarchand F, Sentenac A. Dipole radiation into grating structures. J Opt Soc Am A 2000;17:1048–58.
[39] Weeber J, Hammani K, Colas-des Francs G, et al. Colloidal quantum dot integrated light sources for plasmon mediated photonic waveguide excitation. ACS Photonics 2016;3: 844–52.